DTU Library

High-quality factor, high-confinement microring resonators in 4H-silicon carbide-on-insulator

Zheng, Yi; Pu, Minhao; Yi, Ailun; Chang, Bingdong; You, Tiangui; Huang, Kai; Kamel, Ayman N.; Henriksen, Martin R.; Jørgensen, Asbjørn A.; Ou, Xin

Total number of authors:
11

Link back to DTU Orbit

High-quality factor, high-confinement microring resonators in 4H-silicon carbide-on-insulator

YI ZHENG,[1] MINHAO PU,[1] AILUN YI,[2] BINGDONG CHANG,[3] TIANGUI YOU,[2] KAI HUANG,[2] AYMAN N. KAMEL,[1] MARTIN R. HENRIKSEN,[4] ASBJØRN A. JØRGENSEN,[4] XIN OU,[2] AND HAIYAN OU[1,*]

[1]DTU Fotonik, Technical University of Denmark, Building 343, DK-2800 Lyngby, Denmark
[2]Institute of Microsystem and Information Technology, Chinese Academy of Sciences, 865 Chang Ning Road, Shanghai 200050, China
[3]DTU Danchip, National Center for Micro- and Nanofabrication, Technical University of Denmark, Oersteds Plads, Building 347, DK-2800 Kongens Lyngby, Denmark
[4]Niels Bohr Institute, University of Copenhagen, Blegdamsvej 17, DK-2100 Copenhagen, Denmark
*haou@fotonik.dtu.dk

Abstract: Silicon carbide (SiC) exhibits promising material properties for nonlinear integrated optics. We report on a SiC-on-insulator platform based on crystalline 4H-SiC and demonstrate high-confinement SiC microring resonators with sub-micron waveguide cross-sectional dimensions. The Q factor of SiC microring resonators in such a sub-micron waveguide dimension is improved by a factor of six after surface roughness reduction by applying a wet oxidation process. We achieve a high Q factor (73,000) for such devices and show engineerable dispersion from normal to anomalous dispersion by controlling the waveguide cross-sectional dimension, which paves the way toward nonlinear applications in SiC microring resonators.

1. Introduction

Tremendous effort has been made in the last decade to develop integrated nonlinear platforms using different materials including Si_3N_4 [1], Hydex [2], Diamond [3], AlN [4], AlGaAs [5], etc. Silicon Carbide (SiC) also exhibits promising material properties as a platform for nonlinear applications. Its quadratic ($\chi^{(2)}$) nonlinearity is 30 pm/V [6] and the Kerr nonlinearity is on the order of 10^{-18} m^2/W [7]. Benefiting from the high nonlinearities, different applications have been demonstrated in SiC such as second harmonic generation [8], parametric frequency conversion [9] and self-phase modulation [10]. Besides the large nonlinearities, SiC has a high refractive index (2.6 around 1550 nm), a wide bandgap (2.4 - 3.2 eV depending on different polytypes of SiC [11]) which can avoid two-photon absorption (TPA) at telecom wavelengths (e.g., around 1550 nm), a large transparent window (0.37 - 5.6 μm [12]) and high thermal conductivity (480 $m^{-1}K^{-1}$ [13]). Moreover, point defects in SiC have been exploited for single-photon sources for quantum applications [14, 15].

To realize integrated waveguides in SiC, a thin high quality SiC film should be fabricated with a low-index cladding (e.g. air or glass). Among more than 200 polytypes of different crystalline SiC materials, 3C-, 4H- and 6H-SiC are the common ones which are commercially available. However, 3C-SiC is the most commonly used polytype as it can be epitaxially grown films on silicon substrates, while the others are only available as crystalline bulk wafers. Microresonators are key components for enhancing the efficiency of nonlinear processes [16,17]. SiC/Si microring resonators [18,19] were demonstrated, however, the quality factor (Q) is relatively low (∼ 24000) due to a high material absorption induced by the growth-induced stacking defects. High Qs have so far only been achieved in SiC microdisks [20] and micro-donut resonators [21] where the resonant modes have relatively large effective mode areas (a few square micrometer). For nonlinear processes, not only are high Q microresonators critical, but a small effective

mode area is also desirable for large effective nonlinearity enhancement, which requires small cross-sectional dimensions. Another advantage of high confinement waveguides is flexibility in dispersion engineering. The material dispersion of bulk SiC is normal ($-107\,\mathrm{ps/nm/km}$) at telecom wavelength of 1550 nm. Anomalous dispersion can be readily achieved due to the large index contrast, which is critical for many applications such as Kerr comb generation [22], supercontinuum generation [23, 24], extreme pulse self-compression [25], Raman self-frequency shift [26], etc. However, it is challenging to realize high-confinement waveguides with low loss, because the SiC etching is not a trivial process and the guided light in such waveguides is very sensitive to the surface roughness induced by any fabrication imperfection.

In this paper, we report microring resonators in 4H-silicon carbide-on-insulator (SICOI) realized through the smart-cut technique [27] since 4H-SiC is commercially available and offers higher crystal quality [10]. We applied a wet oxidation process to reduce the surface roughness, which increases the Q by a factor of six. We achieve a Q of 73,000, which is the highest Q achieved in SiC microring resonators with a sub-micron waveguide cross-sectional dimension. The achieved sub-micron dimension enables both strong light confinement and efficient dispersion engineering for SiC waveguides.

2. Device fabrication and characterization

The fabrication process of a SiCOI wafer started from implantation of the 4H bulk SiC wafer with 170 keV H^+ species. H^+ peak concentration was simulated to be at 1.1 μm under the wafer surface. The silicon carrier wafer was then thermally oxidized to grow a 2 μm thick silicon dioxide layer. After cleaning of both wafers, they were bonded together by using direct wafer bonding. The bonded wafers were then annealed at around 850 °C to split the thin SiC film from the bulk SiC wafer. The measured root mean square (RMS) roughness of SiC after splitting is ∼ 5.27 nm, which will induce large scattering for high confinement waveguides. While the roughness of the SiC surface can be reduced by chemical mechanical polishing (CMP) [28]. The linear loss of sub-micron waveguides is also highly dependent on the sidewall roughness, especially for the fundamental transverse electric (TE) mode. To reduce the roughness on both top surface and sidewalls, we applied a wet oxidation processes before and after the SiC waveguide patterning process, leading to significant improvements in surface roughness. Three device samples were fabricated to investigate the influence of the surface roughness on the performance of SiC microring resonators. The SiC layer on sample 1 and sample 2 was thinned down by a dry etching process from 1.1 μm to 500 nm and 600 nm, respectively, while sample 3 was thinned down to 600 nm by a wet oxidation process. Two times six hours' wet oxidation processes were operated at 1100 °C, where the average oxidation rate of SiC was ∼ 0.72 nm/min and hydrofluoric acid was used after each oxidation step to remove SiO_2. The device fabrication on the SiCOI wafers started from electron beam lithography (EBL) with a multi-pass process [29, 30]. A 600 nm thick electron-beam resist layer (hydrogen silsesquioxane) was spun on the SiCOI wafer as the etching mask. The device pattern in the three samples was transferred to the SiC layer in an inductively coupled plasma reactive ion etching (ICP-RIE) machine using fluorine-based gases (SF_6). The selectivity to the etching mask is 1.4 with an etch rate of 140 nm/min. After removing HSQ residues on top of the waveguides, only sample 2 and 3 were applied with an additional wet oxidized for extra two hours to smoothen the waveguide surfaces (incl. the top and sidewall surfaces). This oxidation process also thinned down the SiC waveguide from 600 nm to 500 nm, which made the final waveguide thickness the same in all three samples. Because of the consumption of SiC material in the extra oxidation process, the waveguide widths for sample 2 and sample 3 were designed differently compared to sample 1 at the EBL step in order to have the same final waveguide width. Figures 1(a)–1(c) are atomic force microscopy (AFM) pictures of the SiC waveguide top surfaces of the three samples with the measured RMS roughness being 2.98 nm, 1.34 nm, and 0.72 nm, respectively. In the end, all samples were cladded with SiO_2 by
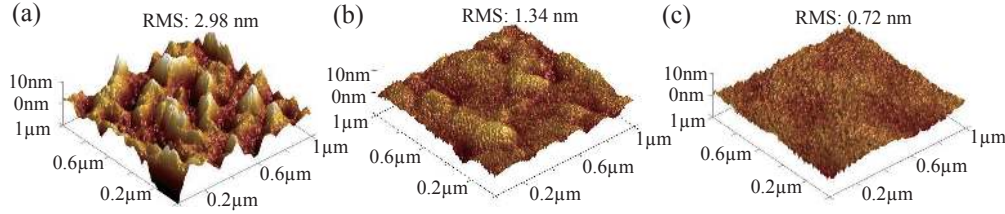
Fig. 1.   AFM pictures of the SiC top surface of three device samples (a) Sample 1: only dry-etching was applied; (b) Sample 2: dry-etching and wet oxidation were applied; (c) Sample 3: wet oxidation was applied both before and after device patterning.

Low-Pressure Chemical Vapor Deposition (LPCVD) followed by Plasma-Enhanced Chemical Vapor Deposition (PECVD).

To test the performance of the devices, microring resonators with a 16.5-μm radius (Fig. 2(a)) were fabricated on the three samples and characterized. Figure 2(b) shows the scanning electron microscope (SEM) picture of the coupling region of a SiC microring resonator with a 175 nm bus-to-ring gap. Figure 2(c) shows the SEM picture of a cross section of a fabricated SiC waveguide, at which the cross-sectional dimension is 750×500 nm^2. The samples were cleaved to form input and output facets, where inverse nano-tapers with 190 nm width tip (linearly tapered from bus waveguide width) enable efficient fiber-to-chip coupling for characterization [31]. Lensed fibers with a spot size of 3.5 μm were used to couple light in and out of the chips and the output was sent to an optical spectrum analyzer (OSA), showing a coupling loss of 3.5 dB/facet across all devices.

Fig. 2. SEM pictures of the fabricated microring resonator with a 16.5-μm radius (a), its coupling region (b) and cross-section of a SiC waveguide (cross-sectional dimension: 750×500 nm^2) (c), where the SiO$_2$ upcladding has been removed.

Figures 3(a) and 3(e) show normalized transmission spectra of the resonators for the fundamental transverse electric (TE) and transverse magnetic (TM) modes, respectively. The insets in Figs. 3(a) and 3(e) are simulated mode profiles with an effective mode area of 0.37 μm^2 and 0.34 μm^2 for fundamental TE and TM modes, where the effective mode areas are 5-10 times smaller than previously reported results [10, 20]. Figures 3(b)–3(d) and 3(f)–3(h) are measured normalized spectra of the TE and TM mode resonances of resonators fabricated under different processes as described in Fig. 1. All devices operated in under-coupled conditions and solid lines show Lorentzian fitting of those resonances. The intrinsic quality factor (Q_{int}) is calculated by using the equation $Q_{int} = 2Q_{load}/(1 + \sqrt{T_0})$ for under-coupled devices [32], where Q_{load} is the measured loaded Q and T_0 is the fraction of transmitted power at resonance wavelength. To extract Q_{int}, we characterized multiple devices for each fabrication condition and found estimated intrinsic Qs for the fundamental TE modes were $(0.9 \pm 0.3) \times 10^4$, $(4.8 \pm 0.2) \times 10^4$ and $(7.1 \pm 0.2) \times 10^4$, respectively. Similarly, the estimated intrinsic Qs for the fundamental
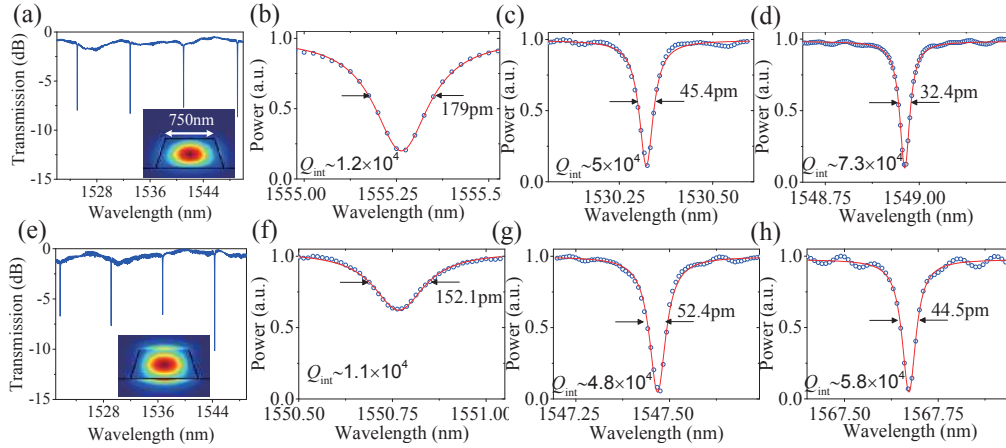
Fig. 3. Measured (normalized) transmission spectra for a 16.5-μm radius microring resonator for the fundamental TE mode (a) and TM mode (e). (b, c, d) and (f, g, h) are resonance fittings for fundamental TE and TM modes of microring resonators fabricated under different processes corresponding to (a, b, c) in Fig. 1. Blue circles are data points and red lines are Lorentzian fitting of those resonances. The insets in (a) and (e) are simulated mode profile of the fundamental TE mode and TM mode, respectively.

TM modes were $(0.9 \pm 0.2) \times 10^4$, $(4.3 \pm 0.5) \times 10^4$ and $(5.4 \pm 0.4) \times 10^4$, respectively. The extracted intrinsic Qs indicate that the applied wet oxidation process not only reduces top surface roughness, but also significantly improves the sidewall roughness of SiC waveguides, leading to an improvement of the Q value of a factor of six, which cannot normally be achieved by CMP. To investigate the loss limit of current devices, we also fabricated 16.5-μm radius microring resonators with waveguide widths of 350 nm and 1065 nm. The extracted intrinsic Qs of TE modes for these microring resonators are $(6.5 \pm 0.3) \times 10^4$ and $(7.5 \pm 0.2) \times 10^4$, respectively. Therefore, we expect that the current loss is mainly due to the material absorption, which could possibly come from the defects produced during implantation. In order to further improve the performance of SiCOI devices, the crystalline quality of the SiC thin film can be improved by H^+ implantation at elevated temperatures [33] or post annealing at a higher temperature to minimize the residual defect losses.

3. Dispersion engineering in high confinement SiC waveguides

Engineering of group velocity dispersion (GVD) is essential for many applications, especially in parametric oscillators or broadband Kerr comb generation [34], where anomalous dispersion with small dispersion slope is desirable [22]. High confinement waveguides are not only beneficial to dispersion engineering due to the large index contrast, but they can also enhance the effective nonlinearity γ, as it is highly dependent on effective mode area as expressed by $2\pi n_2/\lambda A_{\text{eff}}$, where n_2, λ and A_{eff} are the nonlinear refractive index, operation wavelength and effective mode area, respectively. A large effective nonlinearity on the order of $10 \text{ W}^{-1}\text{m}^{-1}$ can be expected in a cross-sectional area of $750 \times 500 \text{ nm}^2$ waveguide. Moreover, only a single to a few modes exist in high confinement waveguides, which can avoid detrimental mode interactions [35]. The dispersion of SiC microring resonators is measured with the experimental setup shown in Fig. 4. The continuous-wave (CW) light was generated by a tunable external-cavity laser (ECL) and split into two paths. The CW light was launched into the SiCOI photonic chip in one path, where the polarization controller (PC) was used to align the output from the lensed fiber to the TE or TM mode of the waveguide. The output from the chip was detected by a photodiode (PD) which was
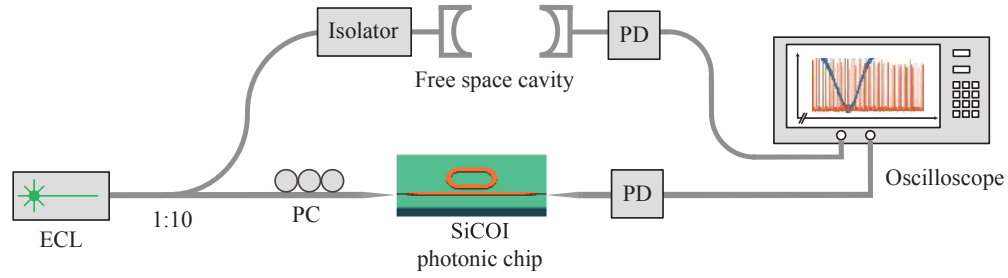
Fig. 4. Schematic view of the dispersion measurement setup for SiCOI microring resonators. The experimental setup consists of the continuous wave generated by an external cavity laser (ECL) coupled to a free space cavity (FSC) and a SiCOI photonic chip through a 1:10 splitter. A polarization controller (PC) is used to adjust the polarization of the output from the lensed fiber. The output of the FSC and the chip are detected by two photodiodes (PDs) which are connected to an oscilloscope.

connected to an oscilloscope. In the other path, the CW light was coupled into a free space cavity (FSC) with 100 MHz free spectral range (FSR) with a finesse around 1000 leading to a linewidth of 100 kHz. An isolator was used to avoid any reflection from FSC to ECL. The output from the FSC was detected by a PD connected to the oscilloscope. The frequency axis was calibrated using the FSC transmission signal, since the dispersion in FSC is very low. The reliability of this method was verified by measuring the GVD of a commercial fiber loop cavity whose GVD value is well known. In this way, the resonant wavelengths of each microring resonator can be determined accurately.

The dispersion of the microring resonator can be obtained by comparing the FSR at different wavelengths. The resonance frequencies of one mode family around ω_0 in a resonator can be approximated as a Taylor expansion [36]:

$$\omega_\mu = \omega_0 + \mu D_1 + \mu^2 D_2/2! + \mu^3 D_3/3! + ... \tag{1}$$

where μ is the relative mode number, $D_1/2\pi$ is the FSR of the microring resonator, D_2 is related to the GVD parameter β_2 as $D_2 = -(c/n)D_1^2\beta_2$, and D_3 and higher are related to higher-order dispersion. To extract the GVD, we measured the transmission of 1004-μm long racetrack microring resonators (consist of 16.5-μm radius curved waveguide and 900-μm long straight waveguide parts) as more resonances exist in such resonators, where more data points can assist better fitting. The integrated dispersion $D_{int}(\mu)$ relative to center wavelength mode at $\mu = 0$ can be expressed as [36]:

$$D_{int}(\mu) = \omega_\mu - (\omega_0 + D_1\mu) = \mu^2 D_2/2! + \mu^3 D_3/3! + ... \tag{2}$$

where $\mu = 0$ is designated to be around 1580 nm in our measurement since scanned wavelength was from 1530 nm to 1630 nm. To show the effects of dispersion engineering, we fabricated 1004-μm long racetrack microring resonators with different widths including 350 nm, 750 nm and 1065 nm while the SiC layer thickness was kept at 500 nm. Figure 5(a) shows the calculated GVD for the fundamental TE (solid) and TM modes (dashed). Circles and triangles are data points of GVD values of the fundamental TE and TM modes at 1580 nm for each waveguide width. Figures 5(b)–5(d) are D_{int} of the fundamental TE mode for 350 nm, 750 nm and 1065 nm wide microring resonators, respectively. Parabolic fits to data points featuring D_2 around -40 MHz, 5 MHz and 3.5 MHz correspond to GVD values around -2010 ps/nm/km, 350 ps/nm/km and 180 ps/nm/km for the fundamental TE mode of waveguide width of 350 nm, 750 nm and 1065 nm, respectively. The GVD of SiC wavguides can be engineered from the normal dispersion regime to anomalous
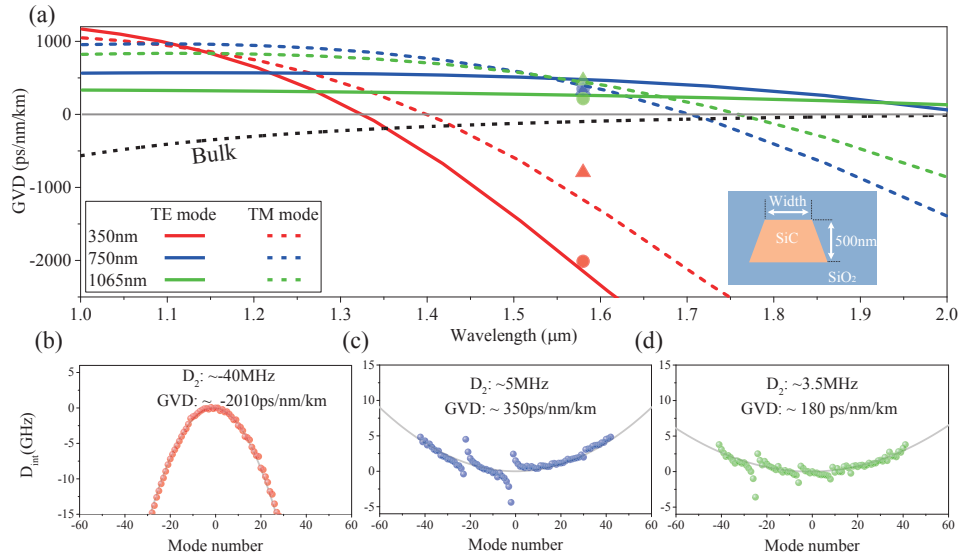
Fig. 5. (a) Calculated GVD of the fundamental TE (solid) and TM mode (dashed) for different waveguide widths. Measured GVD values at 1580 nm for TE (circles) and TM modes (triangles). Measured (colored dots) and fitted (grey curves) are D_{int} of TE modes for waveguide widths of (b) 350 nm, (c) 750 nm and (d) 1065 nm, respectively.

dispersion regime by using different cross-sectional waveguide dimensions. The mode crossings are clearly shown for the waveguide widths of 750 nm and 1065 nm. We believe that the mode crossings come from the interactions between TE and TM mode and such polarization mode crossings could be attributed to the slant sidewall (80° in this case) [37]. All measured GVD values fit well with calculated results when 25 nm waveguide width fabrication variations are taken into account. The GVD measurement shows the dispersion of high confinement SiC waveguides can be tuned from normal dispersion to anomalous, which fulfills the requirements of many nonlinear applications [22, 23, 25, 26].

4.   Conclusion

In conclusion, we report high-Q, high-confinement microring resonators on a SiCOI platform realized through a smart-cut process. The fabrication process has been optimized for this platform, where we obtained an intrinsic Q of 73,000 for microring resonators with sub-micron cross-sectional area. We are able to engineer the dispersion of high confinement SiC waveguides from normal dispersion to anomalous dispersion by tuning the width of the waveguides. The dispersion engineering ability and strong light confinement in such SiC waveguides show promising prospects in efficient nonlinear processes for various applications.

Funding

Acknowledgments

References

1. J. S. Levy, A. Gondarenko, M. A. Foster, A. C. Turner-Foster, A. L. Gaeta, and M. Lipson, "CMOS-compatible multiple-wavelength oscillator for on-chip optical interconnects," Nat. Photonics **4**, 37–40 (2010).
2. L. Razzari, D. Duchesne, M. Ferrera, R. Morandotti, S. Chu, B. Little, and D. Moss, "CMOS-compatible integrated optical hyper-parametric oscillator," Nat. Photonics **4**, 41 (2010).
3. B. J. M. Hausmann, I. Bulu, V. Venkataraman, P. Deotare, and M. Lončar, "Diamond nonlinear photonics," Nat. Photonics **8**, 369–374 (2014).
4. H. Jung, C. Xiong, K. Y. Fong, X. Zhang, and H. X. Tang, "Optical frequency comb generation from aluminum nitride microring resonator," Opt. Lett. **38**, 2810–2813 (2013).
5. M. Pu, L. Ottaviano, E. Semenova, and K. Yvind, "Efficient frequency comb generation in AlGaAs-on-insulator," Optica **3**, 823–826 (2016).
6. I. J. Wu and G. Y. Guo, "Second-harmonic generation and linear electro-optical coefficients of SiC polytypes and nanotubes," Phys. Rev. B **78**, 035447 (2008).
7. R. Adair, L. Chase, and S. A. Payne, "Nonlinear refractive index of optical crystals," Phys. Rev. B **39**, 3337 (1989).
8. S. Yamada, B.-S. Song, S. Jeon, J. Upham, Y. Tanaka, T. Asano, and S. Noda, "Second-harmonic generation in a silicon-carbide-based photonic crystal nanocavity," Opt. Lett. **39**, 1768–1771 (2014).
9. J. Cardenas, S. Miller, Y. Okawachi, S. Ramelow, A. G. Griffith, A. Farsi, A. L. Gaeta, and M. Lipson, "Parametric frequency conversion in silicon carbide waveguides," in CLEO: 2015, (Optical Society of America, 2015), paper SF1D.7.
10. J. Cardenas, M. Yu, Y. Okawachi, C. B. Poitras, R. K. W. Lau, A. Dutt, A. L. Gaeta, and M. Lipson, "Optical nonlinearities in high-confinement silicon carbide waveguides," Opt. Lett. **40**, 4138–4141 (2015).
11. V. Chelnokov and A. Syrkin, "High temperature electronics using SiC: actual situation and unsolved problems," Mater. Sci. Eng. B **46**, 248–253 (1997).
12. S. Wang, M. Zhan, G. Wang, H. Xuan, W. Zhang, C. Liu, C. Xu, Y. Liu, Z. Wei, and X. Chen, "4H-SiC: a new nonlinear material for midinfrared lasers," Laser Photon. Rev. **7**, 831–838 (2013).
13. C. Carter Jr, V. Tsvetkov, R. Glass, D. Henshall, M. Brady, M. St G, O. Kordina, K. Irvine, J. Edmond, H.-S. Kong, R. Singh, S. Allen, and J. Palmour, "Progress in SiC: from material growth to commercial device development," Mater. Sci. Eng. B **61**, 1–8 (1999).
14. S. Castelletto, B. Johnson, V. Ivády, N. Stavrias, T. Umeda, A. Gali, and T. Ohshima, "A silicon carbide room-temperature single-photon source," Nat. Mater. **13**, 151–156 (2014).
15. A. Lohrmann, B. C. Johnson, J. C. McCallum, and S. Castelletto, "A review on single photon sources in silicon carbide," Rep. Prog. Phys. **80**, 034502 (2017).
16. P. Absil, J. Hryniewicz, B. Little, P. Cho, R. Wilson, L. Joneckis, and P.-T. Ho, "Wavelength conversion in GaAs micro-ring resonators," Opt. Lett. **25**, 554–556 (2000).
17. M. Pu, H. Hu, L. Ottaviano, E. Semenova, D. Vukovic, L. K. Oxenløwe, and K. Yvind, "Ultra-efficient and broadband nonlinear AlGaAs-on-insulator chip for low-power optical signal processing," Laser Photon. Rev. **12**, 1800111 (2018).
18. J. Cardenas, M. Zhang, C. T. Phare, S. Y. Shah, C. B. Poitras, B. Guha, and M. Lipson, "High Q SiC microresonators," Opt. Express **21**, 16882–16887 (2013).
19. F. Martini and A. Politi, "Linear integrated optics in 3C silicon carbide," Opt. Express **25**, 10735–10742 (2017).
20. X. Lu, J. Y. Lee, P. X.-L. Feng, and Q. Lin, "High Q silicon carbide microdisk resonator," Appl. Phys. Lett. **104**, 181103 (2014).
21. T. Fan, H. Moradinejad, X. Wu, A. A. Eftekhar, and A. Adibi, "High-Q integrated photonic microresonators on 3C-SiC-on-insulator (SiCOI) platform," Opt. Express **26**, 25814–25826 (2018).
22. T. J. Kippenberg, R. Holzwarth, and S. A. Diddams, "Microresonator-based optical frequency combs," Science **332**, 555–559 (2011).
23. J. K. Ranka, R. S. Windeler, and A. J. Stentz, "Visible continuum generation in air–silica microstructure optical fibers with anomalous dispersion at 800 nm," Opt. Lett. **25**, 25–27 (2000).
24. H. Hu, F. Da Ros, M. Pu, F. Ye, K. Ingerslev, E. P. da Silva, M. Nooruzzaman, Y. Amma, Y. Sasaki, T. Mizuno, Y. Miyamoto, L. Ottaviano, E. Semenova, P. Guan, D. Zibar, M. Galili, K. Yvind, T. Morioka, and L. K. Oxenløwe, "Single-source chip-based frequency comb enabling extreme parallel data transmission," Nat. Photonics **12**, 469–473 (2018).
25. M. A. Foster, A. L. Gaeta, Q. Cao, and R. Trebino, "Soliton-effect compression of supercontinuum to few-cycle durations in photonic nanowires," Opt. Express **13**, 6848–6855 (2005).
26. W. Reeves, D. V. Skryabin, F. Biancalana, J. C. Knight, P. S. J. Russell, F. Omenetto, A. Efimov, and A. Taylor, "Transformation and control of ultra-short pulses in dispersion-engineered photonic crystal fibres," Nature **424**, 511–515 (2003).

27. L. Di Cioccio, Y. Le Tiec, F. Letertre, C. Jaussaud, and M. Bruel, "Silicon carbide on insulator formation using the Smart Cut process," Electron. Lett. **32**, 1144–1145 (1996).
28. L. Zhou, V. Audurier, P. Pirouz, and J. A. Powell, "Chemomechanical polishing of silicon carbide," J. Electrochem. Soc. **144**, L161–L163 (1997).
29. L. Ottaviano, M. Pu, E. Semenova, and K. Yvind, "Low-loss high-confinement waveguides and microring resonators in AlGaAs-on-insulator," Opt. Lett. **41**, 3996–3999 (2016).
30. Y. Zheng, M. Pu, H. K. Sahoo, E. Semenova, and K. Yvind, "High-quality-factor algaas-on-sapphire microring resonators," J. Light. Technol. **37**, 868–874 (2019).
31. M. Pu, L. Liu, H. Ou, K. Yvind, and J. M. Hvam, "Ultra-low-loss inverted taper coupler for silicon-on-insulator ridge waveguide," Opt. Commun. **283**, 3678–3682 (2010).
32. M. Borselli, T. J. Johnson, and O. Painter, "Beyond the rayleigh scattering limit in high-q silicon microdisks: theory and experiment," Opt. Express **13**, 1515–1530 (2005).
33. R. Gregory, T. Wetteroth, S. Wilson, O. Holland, and D. Thomas, "Effects of irradiation temperature and dose on exfoliation of H^+-implanted silicon carbide," Appl. Phys. Lett. **75**, 2623–2625 (1999).
34. T. J. Kippenberg, S. M. Spillane, and K. J. Vahala, "Kerr-nonlinearity optical parametric ocscillation in an ultrahigh-Q toroid microcavity," Phys. Rev. Lett. **93**, 083904 (2004).
35. T. Herr, V. Brasch, J. Jost, I. Mirgorodskiy, G. Lihachev, M. Gorodetsky, and T. Kippenberg, "Mode spectrum and temporal soliton formation in optical microresonators," Phys. Rev. Lett. **113**, 123901 (2014).
36. V. Brasch, M. Geiselmann, T. Herr, G. Lihachev, M. H. Pfeiffer, M. L. Gorodetsky, and T. J. Kippenberg, "Photonic chip–based optical frequency comb using soliton cherenkov radiation," Science **351**, 357–360 (2016).
37. N. Somasiri and B. A. Rahman, "Polarization crosstalk in high index contrast planar silica waveguides with slanted sidewalls," J. Light. Technol. **21**, 54–60 (2003).